Supplementary information

High-throughput bubble screening for rapid design of multi-component alloy catalysts for efficient oxygen evolution

Puchang Hou,[a,b] Ruizhe Ru,[b] Ziyong Zhang,[b] Jinyan Xie,[b] Lei Zhang,[b] Fei Han,[b] Guowei Li,*[b] Jun-Qiang Wan,*[b] and Juntao Huo*[b]

Sample Preparation

We fabricated the target electrocatalysts via a two-stage process combining multi-target co-sputtering for high-throughput screening and single-target magnetron sputtering for fixed-composition synthesis, with dealloying applied in both stages to induce structural reconstruction. For the initial high-throughput composition screening, we selected high-purity metal targets-cobalt (99.95%, Φ50 mm), aluminum (99.999%, Φ50 mm), Fe-Ni alloy (99.95%, Ni:Fe = 50:50 at%, Φ50 mm), and molybdenum (99.95%, Φ50 mm)-and adopted a four-target co-sputtering technique to deposit an Al-Co-Ni-Fe-Mo multicomponent gradient film library on the substrate. We then subject this as-deposited film library to chemical dealloying in 5 M NaOH aqueous solution for 1 h, before conducting rapid OER activity screening with a self-constructed bubble parallel screening setup, which integrates a microscope and a high-resolution camera for real-time monitoring of oxygen bubble evolution during the OER process. For the screening test, we placed the dealloyed film library face down in the electrolyte; the O_2 bubbles generated during OER thus adhered directly to the film surface, and the local bubble volume exhibited a positive correlation with the in-situ OER current density. We captured the real-time differences in bubble size and surface density across distinct regions of the film library via the microscopic imaging system, which allowed us to quickly distinguish the catalytic activity of different compositional regions and establish a direct correlation between elemental composition and OER performance. Through this bubble-assisted screening approach, we finally identified three representative compositional ratios with distinct catalytic activities: the optimal ratio (Al:Co:Ni:Fe:Mo = 32:37.5:8.5:10:12 at%, denoted as Al_{32}/NF), a moderate ratio (29.5:24:13.5:15:8 at%, denoted as $Al_{29.5}$/NF), and a relatively poor ratio (31.5:37:10:11:10.5 at%, denoted as $Al_{31.5}$/NF).

Based on these screening results, we customized multicomponent alloy targets with the three identified ratios, and then prepared fixed-composition catalyst precursors on nickel foam (NF) substrates via single-target magnetron sputtering, with uniform sputtering on both sides of the NF for 4 h to ensure sufficient film loading. To minimize

compositional deviation and ensure the sputtered thin films had a composition highly consistent with the customized targets, we precisely regulated the key sputtering parameters: the background vacuum was maintained at 5×10^{-4} Pa, the argon sputtering pressure at 0.6 Pa, the sputtering power at 80 W, and the substrate temperature at a constant 25°C throughout the deposition process, all of which collectively guaranteed excellent compositional uniformity of the as-sputtered films. We then subjected these fixed-composition NF-supported precursors to a second dealloying treatment in 5 M NaOH for 1 h, a process that induced in-situ topological reconstruction of the catalyst surface and the formation of a well-defined nanosheet structure. This final dealloying step yielded the target dealloyed catalysts, namely D-$Al_{31.5}$/NF, D- $Al_{29.5}$/NF, and D-Al_{32}/NF, completing the entire catalyst preparation workflow.

Material Characterization

Comprehensive structural and compositional characterizations were carried out on the Al-Co-Ni-Fe-Mo sample library and tailored catalysts (Al_{32}/NF, D-$Al_{31.5}$/NF, D-$Al_{29.5}$/NF, D-Al_{32}/NF) before and after dealloying, to clarify structural evolution and elemental distribution changes induced by alkaline treatment. X-ray powder diffraction (XRD, D8 ADVANCE) with a rotating anode was used to identify crystalline phases and compositional characteristics of the entire sample library and individual catalysts. Energy-dispersive X-ray spectroscopy (EDS) mapping and quantitative analysis for the sample library were implemented on a large-chamber scanning electron microscope (SEM, EVO18), while a cold-field emission scanning electron microscope (SEM, S4800) captured detailed surface morphologies of the sample library and catalysts, revealing distinct topological changes before and after dealloying. For cross-sectional and high-resolution structural analysis, thin sections of the sample library and catalysts were prepared via focused ion beam (FIB) milling, a technique critical for preserving original microstructural features, and characterized using a transmission electron microscope (TEM, Talos F200 x) and a cold-field TEM (JEOL F200). Correlative EDS analysis was performed alongside TEM observations to map elemental distribution across both the surface and cross-sections of the samples, establishing a direct link

between structural features and elemental enrichment or leaching. X-ray photoelectron spectroscopy (XPS, Kratos, Axis Ultra DLD) probed the surface chemical states and binding energies of the catalysts, with all XPS spectra calibrated against the adventitious carbon peak (C 1s at 284.5 eV) to eliminate charging effects, a standard calibration step for ensuring valence state analysis accuracy.

Electrochemical Measurements

All electrochemical tests were performed at room temperature in 1 M KOH aqueous electrolyte using a Zahner Zeroge electrochemical workstation with a standard three-electrode configuration. A graphite rod served as the counter electrode, and an Ag/AgCl electrode saturated with 3.5 M KCl was used as the reference electrode; working electrodes were tailored to a fixed geometric size of 1 cm × 0.5 cm for all catalysts, ensuring consistent performance comparison. Oxygen evolution reaction (OER) performance of as-prepared ($Al_{31.5}$/NF, $Al_{29.5}$/NF, Al_{32}/NF) and dealloyed (D-$Al_{31.5}$/NF, D- $Al_{29.5}$/NF, D- Al_{32}/NF) catalysts was evaluated side-by-side to quantify performance enhancement induced by dealloying. Linear sweep voltammetry (LSV) measurements were conducted at a scan rate of 5 mV s^{-1}, and all polarization curves were normalized to the geometric surface area of the working electrode with 95% iR compensation applied to correct for uncompensated solution resistance, a key step for obtaining accurate OER activity data. Electrochemical impedance spectroscopy (EIS) measurements were carried out over a frequency range of 100 mHz to 100 kHz with an AC amplitude of 5 mV, enabling analysis of interfacial charge transfer behavior and reaction kinetics of the OER process.

All measured potentials were converted to the reversible hydrogen electrode (RHE) scale using the Nernst equation (Equation S1), the universal conversion for alkaline electrolyte systems:

$$E_{RHE} = E_{Ag/AgCl} + E_{RF} + 0.0591 \times pH \qquad equ - (S1)$$

Where $E_{Ag/AgCl}$ is the raw potential recorded by the electrochemical workstation,

and E_{RF} is the standard potential of the Ag/AgCl reference electrode (0.2046 V vs. RHE) under the test conditions.

Electrochemical active surface area (ECSA)-a key parameter reflecting the number of exposed catalytic active sites-was determined via cyclic voltammetry (CV) measurements performed in the non-Faradaic potential region at scan rates of 20, 40, 60, 80, and 100 mV s^{-1}. These CV curves were used to estimate the double-layer capacitance (C_{dl}) of the catalysts, a parameter directly proportional to ECSA. The C_{dl} was calculated from the CV data using Equation S2:

$$C_{dl} = \frac{Slope_{anodic} - Slope_{cathodic}}{2} \qquad equ-(S2)$$

where $Slope_{anodic}$ and $Slope_{cathodic}$ represent the linear slopes of the anodic and cathodic current densities plotted against scan rate, respectively, at the midpoint of the non-Faradaic potential window.

ECSA[1] was then calculated from the obtained C_{dl} using Equation S3, with a specific capacitance (C_s) of 0.04 mF cm^{-2}-a widely accepted value for transition metal-based electrocatalysts in alkaline media:

$$ECSA = C_{dl}/C_s \qquad equ-(S3)$$

Quantitative Characterization of OER and Component Screening Based on Bubble Evolution

To achieve the quantitative characterization of OER, a combinatorial characterization method was developed in this study: the sample library was immersed in the electrolyte with its surface facing downward, and a camera was used to in-situ capture the formation behavior of oxygen bubbles on the surface during electrochemical measurements. The bubble volume gradually increased with time during potentiostatic testing, and significant differences in bubble volume and density were observed in different regions of the sample library when the test was paused at a specific time point.

The feasibility of this method was verified through multiple repeated experiments. To establish the quantitative correlation between bubble characteristics and OER activity, the entire bubble image was divided into 60 analytical regions. The diameter of individual bubbles was measured via particle size analysis software, and the volume of single bubbles was calculated using the spherical volume formula, from which the total bubble volume of each region was further derived. A bubble contour map was plotted based on bubble volume and density to realize a direct correspondence between bubble characteristics and catalytic activity-the redder the color of a region, the larger the volume of oxygen generated per unit area and the higher its OER catalytic activity, while a bluer color indicates a weaker OER catalytic activity. To verify the repeatability of bubble formation, the sample library was flipped to release the generated bubbles and then repositioned horizontally with its surface facing upward. It was experimentally observed that a large number of bubbles were still generated in the same regions as those in the first test, which further confirmed the reliability of the correlation between bubble characteristics and catalytic activity.

Based on the correlation between catalytic activity and composition, another sample library of the same specification was also divided into 60 regions. EDS compositional characterization was performed on each region, and the data were collated and summarized to plot a compositional mesh contour map (different colors represent different elemental compositions and contents). By overlaying the compositional mesh with the OER catalytic performance contour map, the structure-activity relationship between OER performance and alloy composition was directly established. Based on the above high-throughput parallel bubble screening method, the composition regions with high OER catalytic activity were successfully screened out in the Al-Co-Ni-Fe-Mo quinary alloy system, and the quantitative correlation mechanism between bubble characteristics and OER activity was fully elucidated. During the EDS compositional analysis and plotting of the compositional mesh map for the sample library, we simultaneously conducted SEM morphological characterization. The results demonstrate that the as-prepared sample library has an overall flat and smooth surface

with no obvious morphological differences.

Criterion and Principle of the High-Throughput Parallel Screening Method

The core criterion of the bubble-based high-throughput screening method in this study is that under the same test conditions, regions with higher OER catalytic activity exhibit faster bubble nucleation, a higher bubble growth rate, and a denser bubble distribution. The fundamental reason for this rule is that the surfaces of high-activity catalysts possess more excellent oxygen generation and desorption kinetic properties. In our experimental system, the electrolyte, applied potential, temperature and other conditions were all strictly controlled to be consistent, which effectively eliminated the interference of interfacial properties, concentration, flow rate and other confounding factors. Therefore, the bubble evolution behavior can reliably and semi-quantitatively reflect the differences in catalytic activity across different regions. Many thanks for your valuable and detailed comment. Compared with traditional electrochemical tests, the advantages of this strategy are as follows: it allows efficient and rapid evaluation of dozens to hundreds of compositions; the catalytic activity can be directly identified according to bubble behavior without sophisticated equipment; and the sample consumption is low, which is especially suitable for the rapid screening of multi-component sample libraries. The limitation is that it is a semi-quantitative screening method, which is more suitable for rapid preliminary screening. Accurate activity data still need to be verified by traditional electrochemical characterizations such as LSV and stability tests. In this study, the strategy of “rapid high-throughput screening + precise electrochemical characterization” is adopted to ensure the reliability of the results. In principle, this bubble-based screening method possesses the potential to be extended to other gas-evolving electrocatalytic reactions, such as HER and overall water splitting. The key rationale is that the method essentially utilizes gas evolution behavior to reflect the catalytic reaction rate. For any electrocatalytic reaction accompanied by obvious bubble formation, higher activity generally leads to faster gas

generation and more vigorous bubble behavior. This study has verified the feasibility using OER as a model reaction. The method can be further extended to other gas-evolving reactions in the future, demonstrating promising potential for universality.

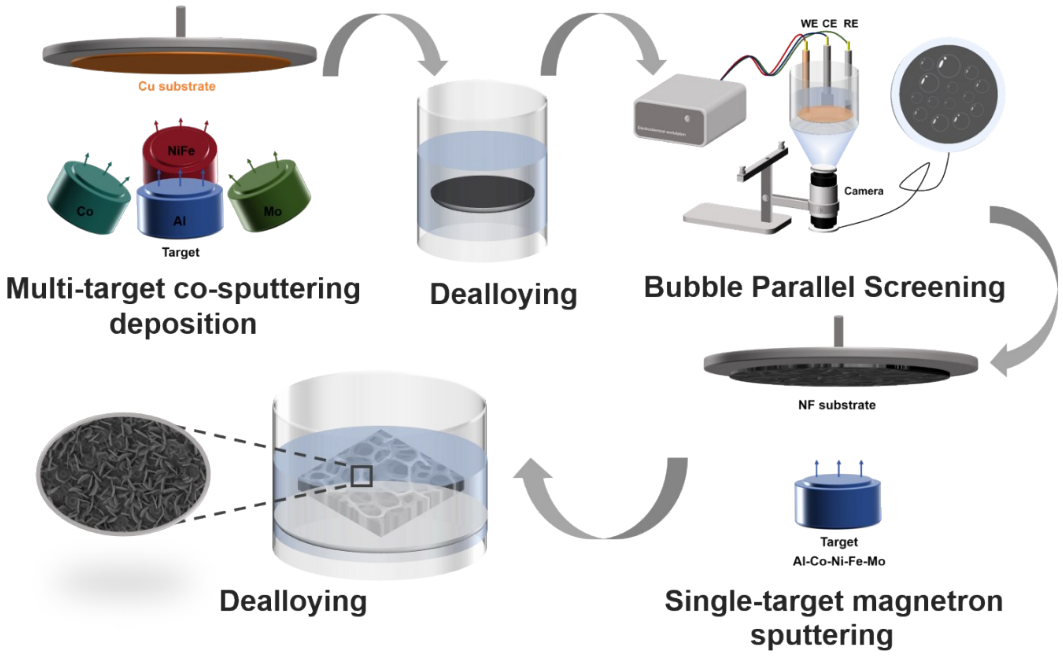

Fig. S1 Schematic diagram of catalyst preparation by the distribution process.

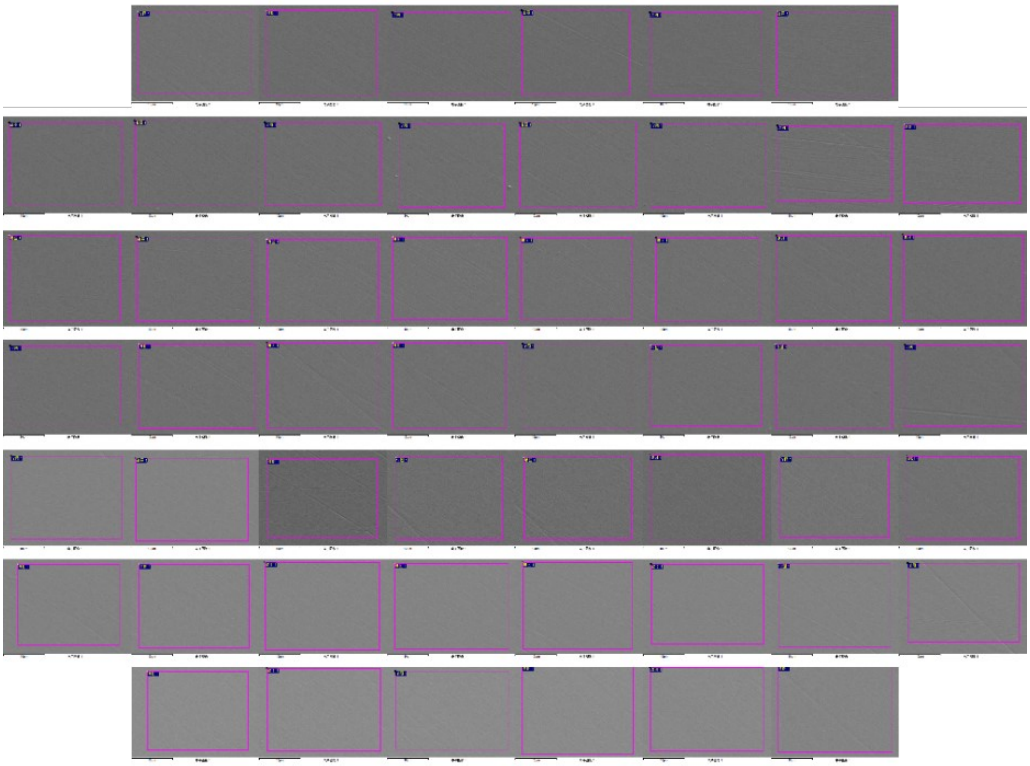

Fig. S2 SEM images of different regions on the sample library.

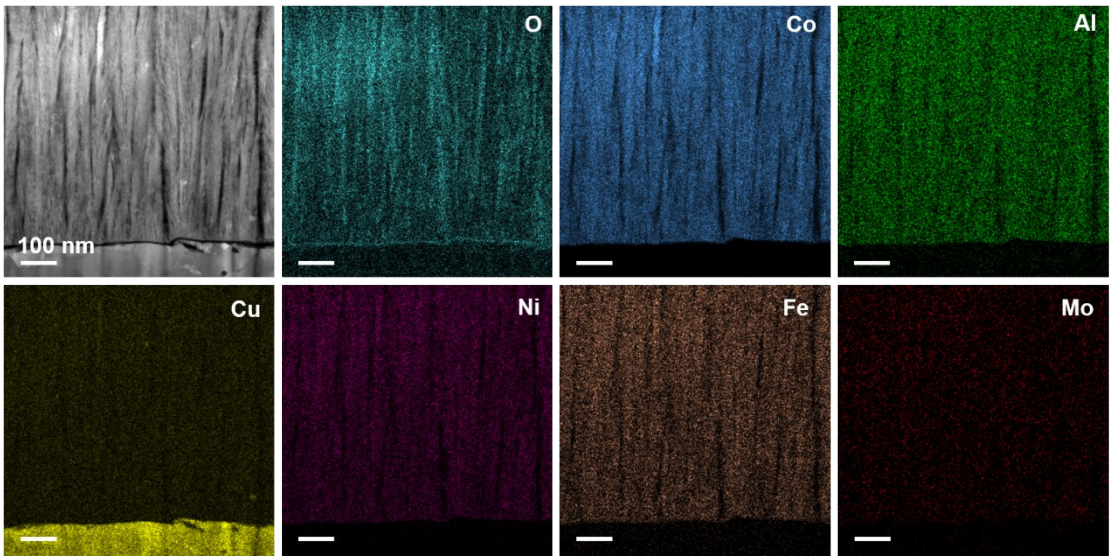

Fig. S3 TEM and EDS images of the as-deposited Al-Co-Ni-Fe-Mo library.

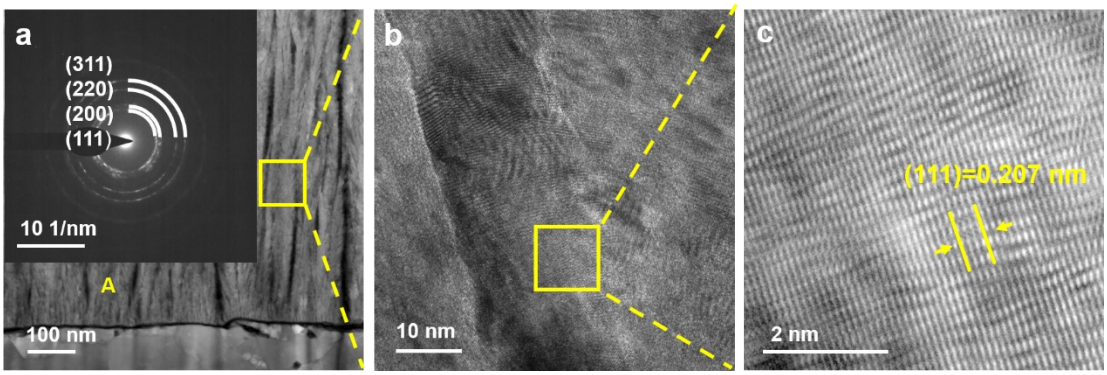

Fig. S4 (a) SAED pattern of the as-deposited Al-Co-Ni-Fe-Mo library. (b) HRTEM image of the as-deposited Al-Co-Ni-Fe-Mo library. (c) Fourier transform pattern.

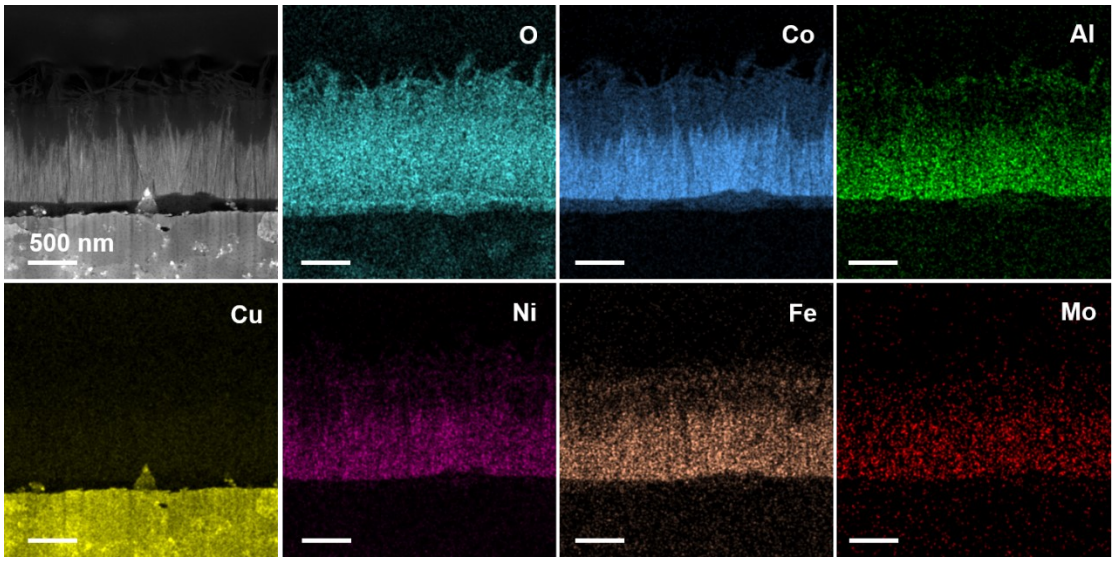

Fig. S5 TEM and EDS images of the dealloyed Al-Co-Ni-Fe-Mo library.

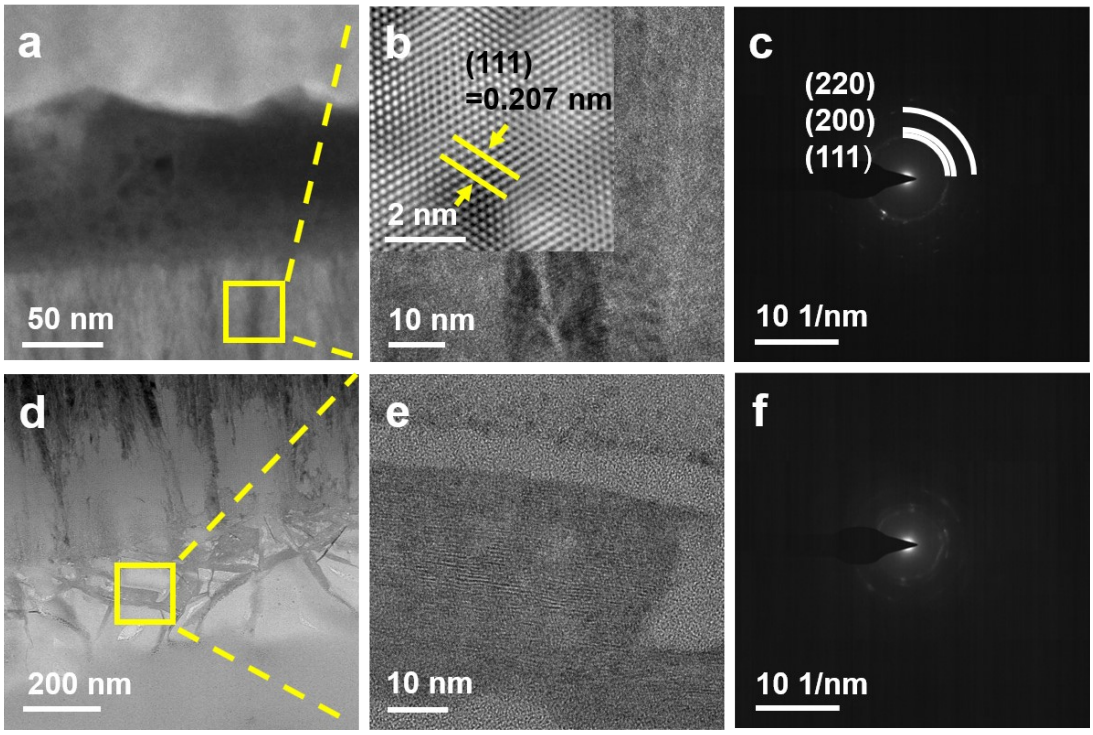

Fig. S6 Structural characterization of the dealloyed Al-Co-Ni-Fe-Mo library. (a) TEM image of the alloyed layer. (b) HRTEM image of the alloyed layer. (c) SAED pattern of the alloyed layer. (d) TEM image of the dealloyed layer. (d) HRTEM image of the dealloyed layer. (f) SAED pattern of the dealloyed layer.

Fig. S7 Bubble distribution map of the sample library.

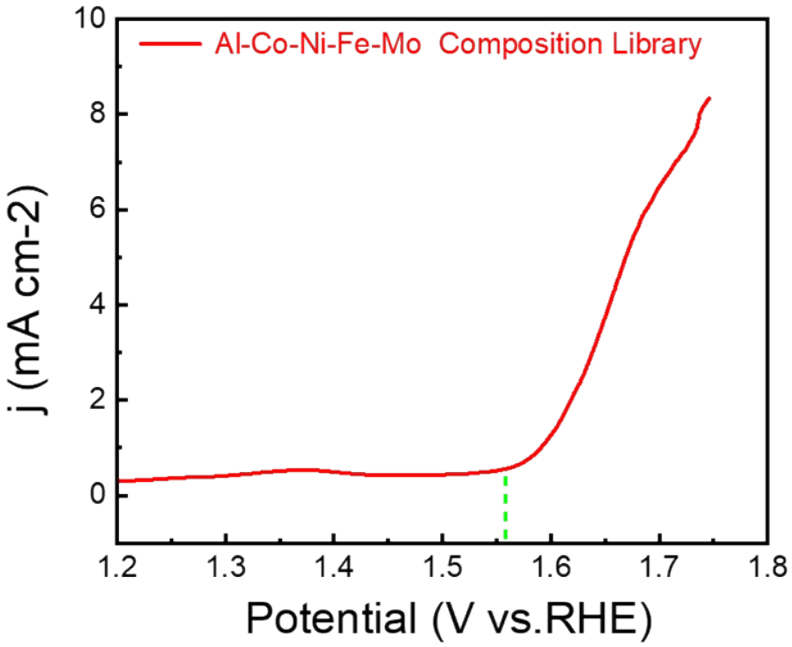

Fig. S8 LSV curves during bubble parallel screening.

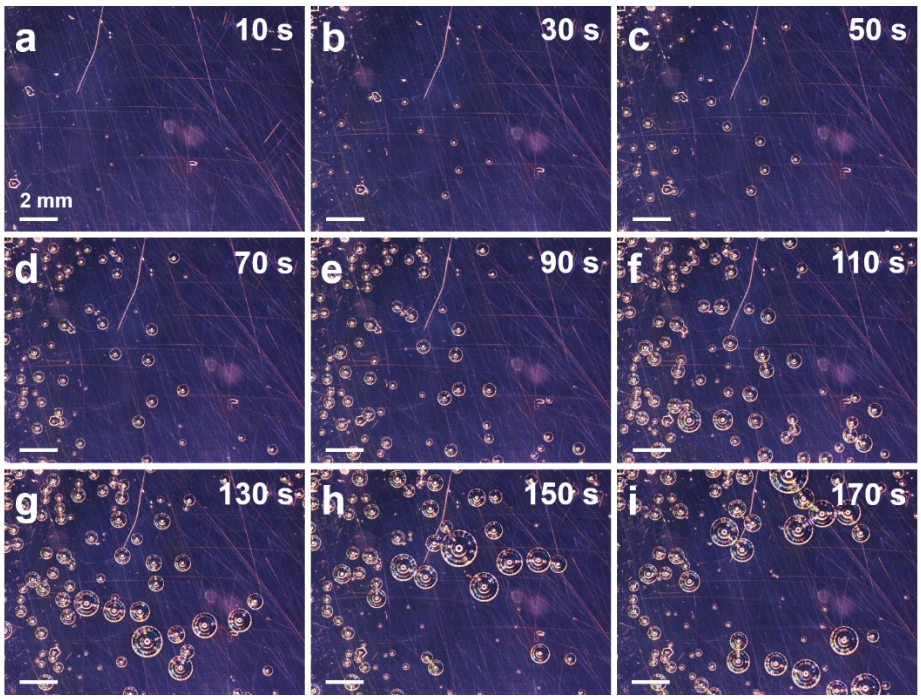

Fig. S9 Optical images of bubbles at the same position at different times.

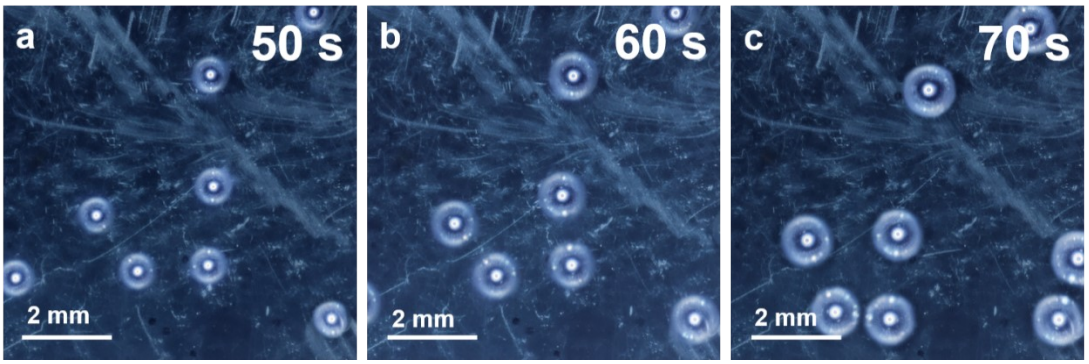

Fig. S10 Optical bubble images at the same position at different times during bubble parallel screening.

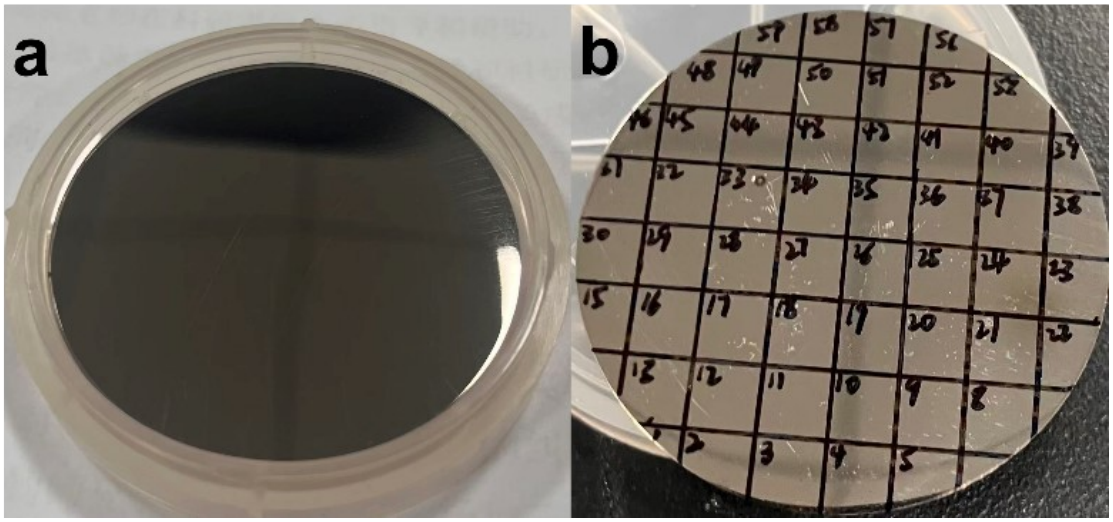

Fig. S11 (a-b) the sample library fabricated by magnetron sputtering deposition.

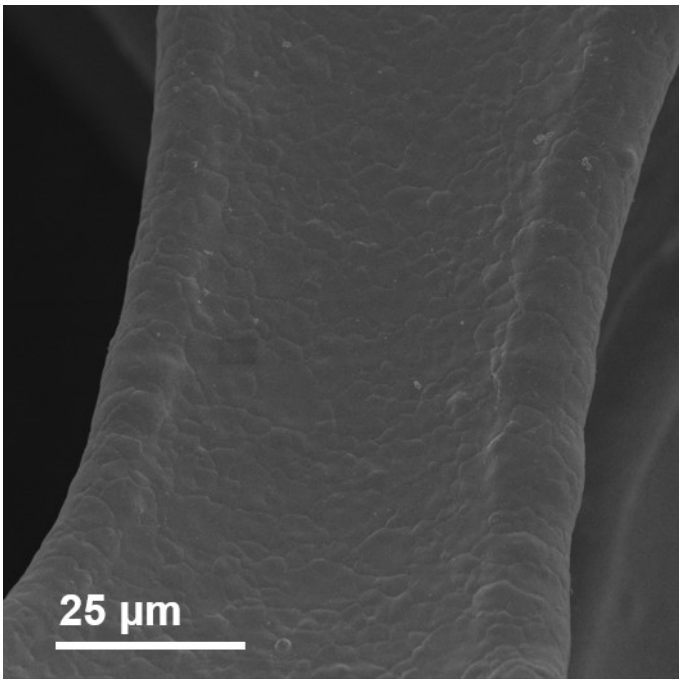

Fig. S12 SEM image of the pristine Al_{32} sample.

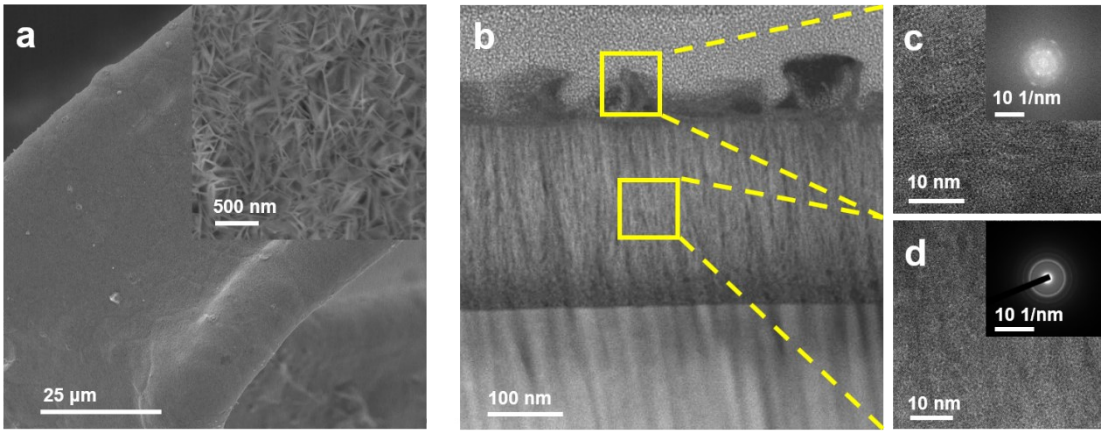

Fig. S13 Structural characterization of the dealloyed $A_{31.5}$ sample. (a) SEM image. (b) TEM image. (c) HRTEM image of the nanosheet layer. (d) HRTEM image of the nano-precursor layer.

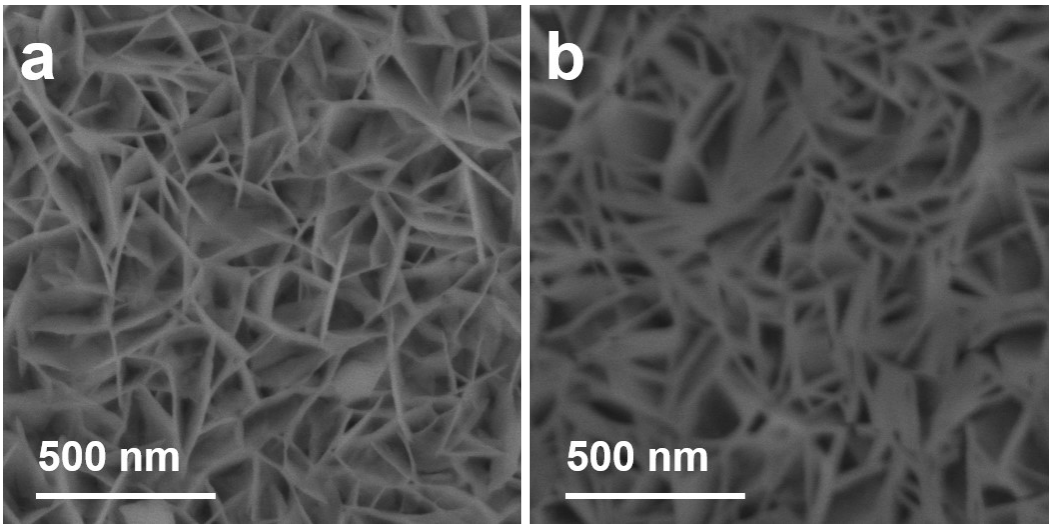

Fig. S14 SEM images of the samples after the stability test at 10 mA cm^{-2}. (a) SEM image of D-Al_{32}/NF (b) SEM image of D-$Al_{31.5}$/NF.

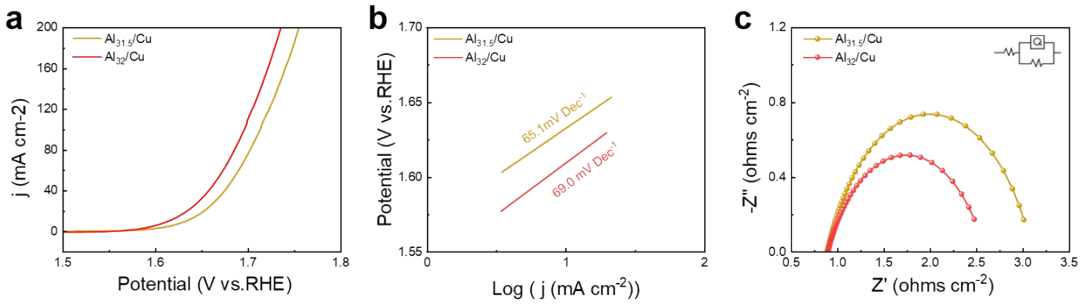

Fig. S15 (a) OER polarization curves. (b) Tafel slopes. (c) Nyquist plots.

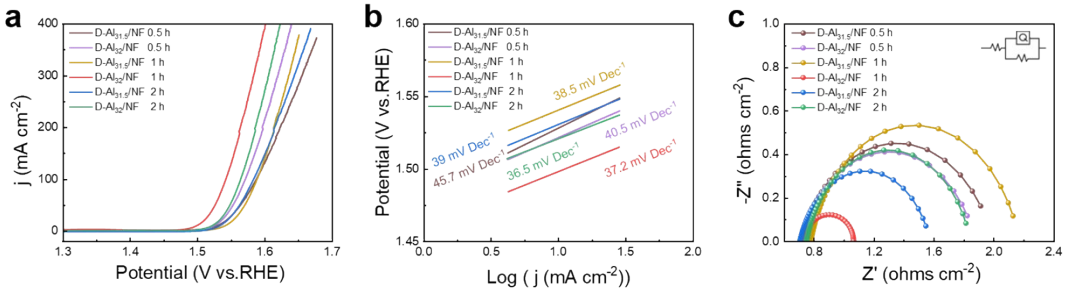

Fig. S16 (a) OER polarization curves. (b) Tafel slopes. (c) Nyquist plots.

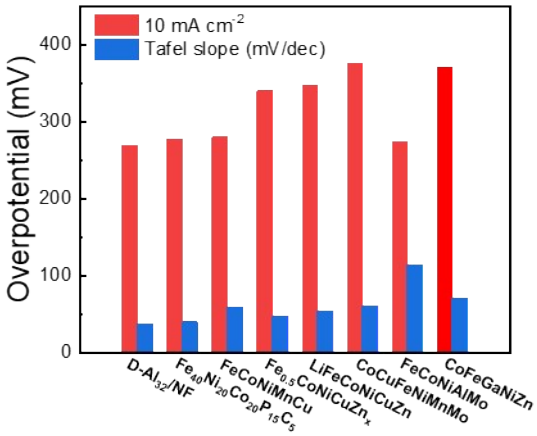

Fig. S17 Comparison of OER performance among recent multicomponent alloy electrocatalysts.

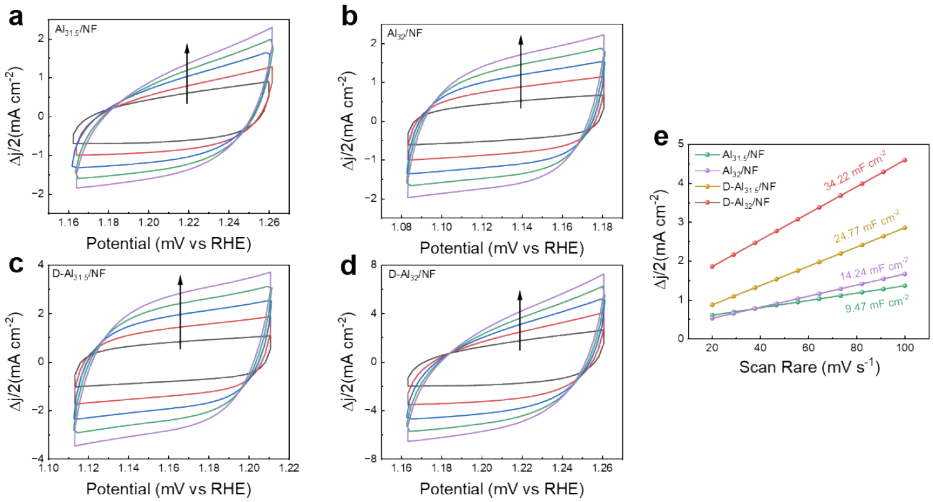

Fig.S18 (a-d) CV curves of $Al_{31.5}$/NF, Al_{32}/NF, D-$Al_{31.5}$/NF, and D-Al_{32}/NF samples. (e) Capacitance current as a function of scan rate.

Table 1 Comparison of OER performance of recent multicomponent alloy electrocatalysts

OER Catalyst	Electrolyte (1.0 M)	Overpotential (@ 10 mA cm^{-2})	Tafel Slope (mV/dec)	Stability (10 mA cm^{-2})	Reference
D-Al_{32}/NF	KOH	269 mV	37.1	100 h	
$Fe_{40}Ni_{20}Co_{20}P_{15}C_5$	KOH	278 mV	40	20 h	[2]
FeCoNiMnCu	KOH	280 mV	59	40 h	[3]
$Fe_{0.5}CoNiCuZn_x$	KOH	340 mV	48	24 h	[4]
LiFeCoNiCuZn	KOH	347 mV	53.8	20 h	[5]
CoCuFeNiMnMo	KOH	375 mV	61	72 h	[6]
FeCoNiAlMo	KOH	274 mV	114.49	0.5 h	[7]
CoFeGaNiZn	KOH	370 mV	71	10 h	[8]

References

1. Pan, M.; Feng, H.; Zhang, Z.; Gao, M.; Lei, L.; Wang, D.; Li, G.; Huo, J.; Wang, J.-Q., Observation of a robust catalyst support based on metallic glass for large current-density water electrolysis. *Journal of Materials Chemistry A* 2024, *12* (25), 15334-15342.

2. Aneeshkumar, K. S.; Tseng, J.-c.; Liu, X.; Tian, J.; Diao, D.; Shen, J., Electrochemically dealloyed nanoporous $Fe_{40}Ni_{20}Co_{20}P_{15}C_5$ metallic glass for efficient and stable electrocatalytic hydrogen and oxygen generation. *RSC Advances* 2021, *11* (13), 7369-7380.

3. Chen, W.; Hu, C.; Li, J.; He, S.; Liu, H.; Hua, Z., Oxygen Evolution Enhancement of Bulk FeCoNiAlMo High-Entropy Alloy through Electrochemical Dealloying in ChCl-EG Deep Eutectic Solvent. *Langmuir* 2025, *41* (22), 14345-14359.

4. Huang, K.; Peng, D.; Yao, Z.; Xia, J.; Zhang, B.; Liu, H.; Chen, Z.; Wu, F.; Wu, J.; Huang,

Y., Cathodic plasma driven self-assembly of HEAs dendrites by pure single FCC FeCoNiMnCu nanoparticles as high efficient electrocatalysts for OER. *Chemical Engineering Journal* 2021, *425*.

5. Huang, J.; Wang, P.; Li, P.; Yin, H.; Wang, D., Regulating electrolytic Fe0.5CoNiCuZn high entropy alloy electrodes for oxygen evolution reactions in alkaline solution. *Journal of Materials Science & Technology* 2021, *93*, 110-118.

6. Gu, Y.; Bao, A.; Wang, X.; Chen, Y.; Dong, L.; Liu, X.; Pan, H.; Li, Y.; Qi, X., Engineering the oxygen vacancies of rocksalt-type high-entropy oxides for enhanced electrocatalysis. *Nanoscale* 2022, *14* (2), 515-524.

7. Asghari Alamdari, A.; Jahangiri, H.; Yagci, M. B.; Igarashi, K.; Matsumoto, H.; Motallebzadeh, A.; Unal, U., Exploring the Role of Mo and Mn in Improving the OER and HER Performance of CoCuFeNi-Based High-Entropy Alloys. *ACS Applied Energy Materials* 2024, *7* (6), 2423-2435.

8. Sharma, L.; Katiyar, N. K.; Parui, A.; Das, R.; Kumar, R.; Tiwary, C. S.; Singh, A. K.; Halder, A.; Biswas, K. J. N. R., Low-cost high entropy alloy (HEA) for high-efficiency oxygen evolution reaction (OER). 2022, *15* (6), 4799-4806.